Structure of chemically synthesized nanophase GaAs studied by nuclear magnetic resonance and x-ray diffraction

L. D. Potter
Department of Physics and Astronomy, University of North Carolina, Chapel Hill, North Carolina 27599

A. A. Guzelian and A. P. Alivisatos
Department of Chemistry, University of California, Berkeley, California 94720

Y. Wu
Department of Physics and Astronomy, University of North Carolina, Chapel Hill, North Carolina 27599

(Received 16 May 1995; accepted 20 June 1995)

Nanophase GaAs produced by organometallic synthesis was studied by ^{71}Ga, ^{69}Ga, and ^{75}As nuclear magnetic resonance (NMR) as well as x-ray diffraction. The structure of the samples synthesized below 250 °C is predominantly amorphous. Raising the temperature of synthesis (or post-synthesis annealing) above 280 °C improves significantly the crystallinity as evidenced by the appearance of a sharp bulklike ^{71}Ga (and ^{69}Ga) peak. In addition, a sharp peak shifted up-field also appears. Other NMR features of this up-field shifted peak are very similar to the bulklike peak including quadrupole interactions and spin–lattice and spin–spin relaxations. These results are consistent with the presence of stacking faults in nanocrystalline GaAs.

I. INTRODUCTION

Semiconductor nanocrystals exhibit a wide variety of intriguing size-dependent properties, such as the blue shift of the optical absorption and photoluminescence, electronic and nonlinear optical effects, as well as structural effects such as increased solid–solid phase transition pressures.[1] These properties are also influenced strongly by surface effects and defects which are sensitive to the method of fabrication. In addition, the large surface area and the specific growth kinetics can also influence the interior structure of nanocrystals. It is not obvious that the interior structure of a nanocrystal should be identical to the corresponding bulk material. It was found, for instance, that CdTe nanocrystals have predominantly wurtzite structure unlike the structure of bulk CdTe which is zincblende.[2] Structural deviations from bulk materials may also arise from defects in nanocrystals; stacking faults were clearly identified in high quality CdSe nanocrystals.[2] Evidence of stacking faults in nanocrystalline GaN has also been found.[3] X-ray diffraction (XRD) is the primary technique for studying the lattice structure of nanocrystals. However, because of the short coherence length imposed by the intrinsic small size of nanocrystals, diffraction peaks are broadened significantly. Consequently, XRD may fail to reveal some subtle structural features of small nanocrystals. For example, simulation shows that with a small number of stacking faults wurtzite CdSe nanocrystals exhibit qualitatively similar diffraction patterns as zincblende CdSe nanocrystals.[2] Similar phenomena were observed in nanocrystalline GaN.[3] Thus, as complementary techniques to XRD, site-specific local probes such as nuclear magnetic resonance (NMR) can be quite valuable in characterizing structures of nanocrystals.[4–7] For the same reason, NMR can be very useful in characterizing structures of nanophase materials where both the growth kinetics and the presence of substantial grain boundaries and disordered regions may have a significant effect on the structure.

Techniques of chemical synthesis have been developed over the last decade for making soluble noninteracting semiconductor nanocrystals of II–VI materials including CdS, CdSe, and CdTe.[2,8] Nanophase GaAs and soluble noninteracting GaAs nanoparticles have also been synthesized.[9–13] In this work, we report ^{71}Ga, ^{69}Ga, and ^{75}As solid-state NMR and XRD studies of nanophase GaAs obtained by organometallic synthesis. In samples synthesized or annealed at temperatures above 280 °C two narrow ^{71}Ga (and ^{69}Ga) resonance peaks with comparable intensities can be resolved under magic angle spinning (MAS). Both peaks correspond to tetrahedrally coordinated gallium sites. One resonance peak has a chemical shift of 210 ppm which is very close to the 217 ppm chemical shift of the single peak observed in bulk GaAs; the other peak is at 183 ppm. Except for the different chemical shifts, the two peaks exhibit similar properties: The small quadrupole interactions indicate slight distortions from cubic symmetry; the identical spin–lattice and spin–spin relaxation rates indicate analogous local environments while the identical spin–spin relaxation rates also imply closely related electronic structures. These similar properties suggest that only subtle structural differences distinguish these two sites. A model of the lattice structure consistent with the available NMR and x-ray data includes stacking faults in the nanocrystalline domains. These faults would give rise to both cubic and hexagonal close-packed layers with the latter corresponding to the 183 ppm peak.

II. EXPERIMENT

Nanophase GaAs powders were produced by chemical reactions of $GaCl_3$ with tris(trimethylsilyl) arsine ($As(SiMe_3)_3$) carried out in various solvents including quinoline, hexadecane, and trioctyl amine.[9,10,12] The reaction temperature was 230 °C in the quinoline solvent, 290 °C in the trioctyl amine solvent, and 100 °C to 285 °C in the hexadecane solvent; the nanophase GaAs powders were obtained upon removal of the solvent. A sample of the nanophase GaAs powders made in quinoline was flame-annealed in

 0021-9606/95/103(12)/4834/7/$6.00

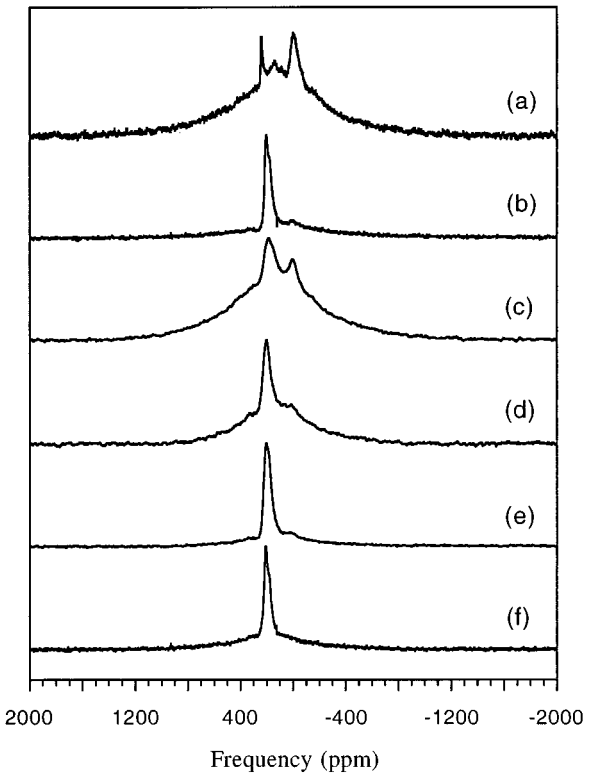

FIG. 1. ^{71}Ga MAS spectra of chemically synthesized GaAs. Preparation conditions: (a) and (b) quinoline solvent, reaction temperature of 230 °C, and the latter flame-annealed at 450 °C; (c), (d), and (e) hexadecane solvent, reaction temperatures of 190 °C, 250 °C, and 285 °C, respectively; (f) trioctyl amine solvent, reaction temperature of 290 °C. The spectra were obtained from the Hahn-echo pulse sequence as explained in the text with 1.4–2.3 μs $\pi/2$ pulses and with MAS rotation frequencies between 16 and 18 kHz.

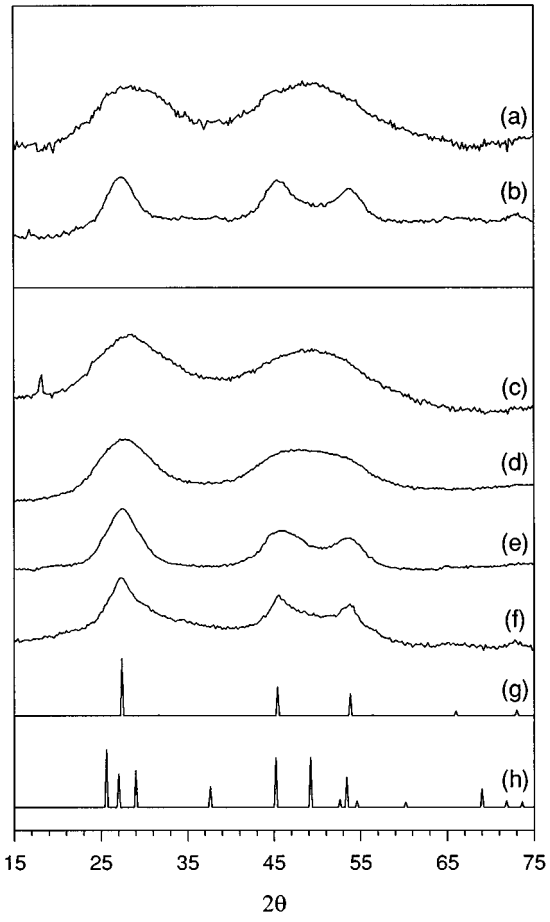

FIG. 2. Powder XRD spectra of chemically synthesized GaAs. (a) Prepared in quinoline at 230 °C, domain size 11 Å, (b) prepared in quinoline and then flame-annealed at 450 °C, domain size 25 Å; (c) prepared in hexadecane at 190 °C, domain size 13 Å; (d) prepared in hexadecane at 250 °C, domain size 15 Å; (e) prepared in hexadecane at 285 °C, domain size 24 Å; prepared in trioctyl amine at 290 °C, domain size 30 Å; (g) calculated zincblende GaAs XRD spectrum; (h) calculated wurtzite GaAs XRD spectrum.

vacuum at 450 °C before exposure to air. The powders consist mainly of insoluble macroscopic GaAs particles; these particles are nanophase GaAs according to XRD as will be discussed later. The Ga to As molar ratio is 1:1 in all samples as obtained by elemental analysis. Powder XRD spectra were obtained on a Siemens D5000 diffractometer using Cu Kα radiation.

The room temperature NMR experiments were carried out on a Chemagnetics CMX400 pulsed spectrometer at 9.4 Tesla. High-resolution spectra were obtained by MAS.[14] The ^{71}Ga and ^{69}Ga resonances in dilute aqueous gallium nitrate solution were used as shift references for ^{71}Ga and ^{69}Ga whereas the shift of ^{75}As resonance in bulk GaAs was used as the shift reference for ^{75}As. The Hahn-echo technique was used to detect broad resonance lines. The $\pi/2$ tipping and the π refocusing pulses were synchronized with the rotor of the MAS probe when the Hahn-echo technique was combined with MAS. The $1/2 \leftrightarrow -1/2$ central transition was selectively excited using $\mathscr{H}_{\rm rf} \ll \mathscr{H}_Q^1$ where $\mathscr{H}_{\rm rf} = \omega_{\rm rf} I_x$ is the rf term and $\mathscr{H}_Q^1$ represents the first-order quadrupole interaction.[14,15]

III. RESULTS AND DISCUSSION

Figure 1(a) shows the ^{71}Ga MAS spectrum of the $1/2 \leftrightarrow -1/2$ central transition obtained from the as-synthesized nanophase GaAs powder made in quinoline. Two narrow lines and one broad line can be identified. The very narrow peak at 250 ppm is due to an unknown Ga complex as evidenced by the significant reduction of the peak intensity after the sample was washed with toluene. The narrow peak at 0 ppm originates from oxidation upon exposing the sample to air as will be discussed later. The broad peak, centered around 150 ppm, is attributed to nanophase GaAs. The XRD pattern of this sample, shown in Fig. 2(a), is qualitatively different from the one of zincblende structure; the expected (220) and (311) diffraction peaks of the zincblende structure cannot be resolved. The domain size of the crystallites in the sample can be estimated from the Debye–Scherrer formula given by

$$\Delta(2\theta) = \frac{1.2\lambda}{D \cos \theta}, \tag{1}$$

where D is the domain size, Δ is the width of the diffraction peak, λ is the x-ray wavelength, and θ is the Bragg angle.[16] The broad linewidth of the diffraction peaks in Fig. 2(a) implies a very small domain size of 11 Å, indicating that the structure of this as-synthesized nanophase GaAs material is

highly disordered. It is plausible to attribute the line broadening of the 150 ppm peak to structural disorder. This is consistent with the fact that no ^{75}As signal can be observed in this sample. Because of the large quadrupole moment, ^{75}As is very sensitive to local disorder. Large second-order quadrupolar line broadening in noncubic local environments makes the detection of the ^{75}As signal very difficult in highly disordered systems.

The crystallinity of the nanophase GaAs powder made in quinoline was improved significantly upon flame annealing.[10] This is evidenced by XRD as shown in Fig. 2(b). The diffraction peaks are sharper compared to the as-synthesized sample, and the estimated domain size increases to 25 Å. Also, the (220) and (311) peaks can be clearly resolved as each peak narrows around the bulk GaAs zincblende positions. However, recent studies have shown that the broadening of these peaks due to the small size of the nanocrystalline domains can mask the effect of subtle structural features such as stacking faults.[2,3] As a probe of local structure, NMR should reveal such features. Figure 1(b) shows the ^{71}Ga MAS spectrum of the flame-annealed sample; a similar MAS spectrum was observed for ^{69}Ga. An intense sharp peak around 200 ppm, which is absent in Fig. 1(a), appears in both ^{71}Ga and ^{69}Ga spectra. The broad peak at 150 ppm in Fig. 1(a) is reduced significantly as expected from the improved crystallinity. For comparison, the ^{71}Ga MAS spectrum of a bulk GaAs sample is shown in Fig. 3(a). A single symmetric peak is observed at 217 ppm; the linewidth at half height $\Delta\nu_{1/2}$ is 1.54 kHz which remains constant above a MAS rotation frequency of a few kHz. In order to display detailed features of the peak around 200 ppm in Fig. 1(b), the ^{71}Ga MAS and ^{69}Ga MAS spectra of the flame-annealed sample are plotted in Figs. 3(b) and 3(c), respectively. In contrast to the featureless spectrum of bulk GaAs, there are clearly two resonance peaks, labeled *a* and *b*, in both the ^{71}Ga and ^{69}Ga MAS spectra. The fact that the fine features represent two different peaks rather than a residual second-order quadrupolar powder pattern is demonstrated below.

Under MAS the only remaining anisotropic broadening is the residual second-order quadrupolar broadening.[17,18] This results in an anisotropic resonance frequency ν_{aniso} for the $1/2 \leftrightarrow -1/2$ central transition. ν_{aniso} can be described as[19–21]

$$\nu_{\text{aniso}} = \left(\frac{\nu_Q}{2I(2I-1)}\right)^2 \frac{4I(I+1)-3}{32\nu_L} f_\eta(\alpha,\beta), \tag{2}$$

where I is the spin quantum number of the nucleus, ν_L is the Larmor frequency, $\nu_Q = e^2Qq/h$ is the quadrupole coupling constant, and $f_\eta(\alpha,\beta)$ depends only on the asymmetry parameter η of the electric field gradient (EFG) tensor and the polar angles α and β of the crystallite with respect to the spinner axis. The effect of ν_{aniso} is more significant for ^{69}Ga than ^{71}Ga spectra because of the larger quadrupole moment Q and the lower Larmor frequency of ^{69}Ga. In ppm unit the ^{69}Ga powder pattern can be obtained by scaling the ^{71}Ga powder pattern with the factor $[Q^2(^{69}\text{Ga})\nu_L^2(^{71}\text{Ga})]/[Q^2(^{71}\text{Ga})\nu_L^2(^{69}\text{Ga})]=4$. This is clearly not the case for the two-peak feature of the MAS spectra shown in Figs. 3(b) and 3(c). Therefore, this feature of the MAS spectra in Figs. 3(b) and 3(c) results from two peaks corresponding to two different local environments with different isotropic chemical shifts.

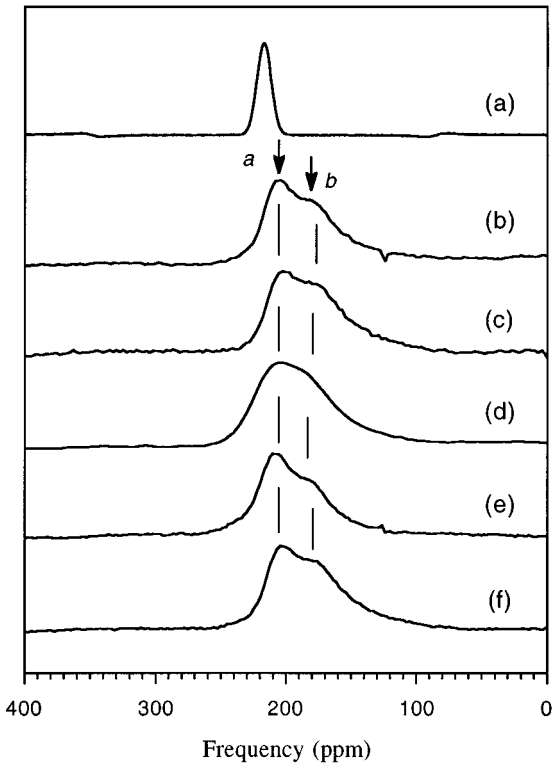

FIG. 3. (a) ^{71}Ga MAS spectrum of bulk GaAs. (b) ^{71}Ga and (c) ^{69}Ga MAS spectra of GaAs made in quinoline and flame-annealed at 450 °C. (d) ^{71}Ga MAS spectrum of GaAs made in hexadecane at 280 °C. (e) ^{71}Ga and (f) ^{69}Ga MAS spectra of GaAs made in trioctyl amine at 290 °C. The spectrum in (a) was obtained from the free induction decay after a 5 μs $\pi/2$ pulse and with a MAS rotation frequency of 16 kHz. The other spectra were obtained from the Hahn-echo pulse sequence with 1.4–2.3 μs $\pi/2$ pulses and with sample rotation frequencies between 15 and 18 kHz.

Unlike bulk GaAs, neither peak *a* nor peak *b* corresponds to perfect cubic environments. The $\pi/2$ pulse in bulk GaAs is precisely twice longer than the effective $\pi/2$ pulse for peaks *a* and *b*. This indicates that only the central transition is excited in nanophase GaAs samples because of quadrupolar broadening.[17] Since neither peak *a* nor peak *b* exhibit characteristic features of the residual second-order quadrupolar powder pattern, the asymmetry parameter η of the corresponding EFG tensors for peaks *a* and *b* cannot be determined. It is well known that isotropic indirect couplings, which cannot be removed by MAS, are strong in bulk GaAs;[22] the 1.54 kHz linewidth of the ^{71}Ga MAS spectrum in Fig. 3(a) can be accounted for entirely by the heteronuclear isotropic indirect couplings between ^{71}Ga and ^{75}As nuclei.[23] In addition, a distribution of local environments, which are expected in nanophase GaAs, contributes to the linewidths. Thus, the linewidths of peaks *a* and *b* cannot be used as reliable measures of quadrupolar broadenings. In fact, the linewidths of peaks *a* and *b* are not much larger than that of bulk GaAs. The quantity $\nu_Q\sqrt{1+\eta^2/3}$ associated with peaks *a* and *b* can be estimated from the differ-

TABLE I. Chemical shifts and quadrupole parameters for the indicated samples. The observed shifts δ_e of peaks *a* and *b*, obtained from the ^{71}Ga and ^{69}Ga spectra, were used to determine the quantity $\nu_Q\sqrt{1+\eta^2/3}$ and the isotropic chemical shift δ_c for each peak.

		δ_e (ppm)		$\nu_Q\sqrt{1+\frac{\eta^2}{3}}$ (MHz)		δ_c (ppm)	
		a	*b*	*a*	*b*	*a*	*b*
GaAs made in quinoline and flamed	^{71}Ga	208	181	0.98	0.98	210	183
	^{69}Ga	203	176	1.6	1.6		
GaAs made in trioctyl amine	^{71}Ga	209	182	0.98	0.98	211	184
	^{69}Ga	204	177	1.6	1.6		

ences of the observed isotropic shifts δ_e, listed in Table I, between the ^{71}Ga and ^{69}Ga spectra. This is based on the existence of the isotropic second-order quadrupolar shift given by[17] (in ppm)

$$\delta_i = -\frac{3\times10^5}{4}\frac{\nu_Q^2}{\nu_L^2}\left(1+\frac{\eta^2}{3}\right)\frac{[I(I+1)-3/4]}{I^2(2I-1)^2}. \tag{3}$$

It depends on $\nu_Q\sqrt{1+\eta^2/3}$ and ν_L which are different for ^{71}Ga and ^{69}Ga. Table I lists the derived $\nu_Q\sqrt{1+\eta^2/3}$ values which are the upper limits of the corresponding ν_Q values. The isotropic chemical shift δ_c, as determined from $\delta_e=\delta_c+\delta_i$, is also listed in Table I for both peak *a* and *b*. The chemical shift of 210 ppm for peak *a* is very close to the value of 217 ppm in bulk GaAs, and the peak *b* is shifted upfield to 183 ppm which is also in the chemical shift region of tetrahedrally coordinated Ga. The upper limit of the ^{71}Ga quadrupole coupling constant is only about 1 MHz for both peak *a* and *b*; according to powder pattern simulations, the contribution of such quadrupole interactions to the linewidth of ^{71}Ga MAS spectra taken at 9.4 Tesla is only about a few ppm, which is consistent with the narrow linewidths of peaks *a* and *b*. Simulating the two peaks with Lorentzian peaks yields an intensity ratio of peak *a* to peak *b* of 1.2.

Figures 1(c), 1(d), and 1(e) show ^{71}Ga MAS spectra of a series of nanophase GaAs samples synthesized in hexadecane at 190 °C, 250 °C, and 280 °C, respectively. Again, the oxide peak at 0 ppm is present, especially in samples synthesized at low temperatures. The broad peak around 150 ppm is also present. The intensity of this broad peak, however, is reduced dramatically in samples synthesized above 250 °C. Figures 2(c), 2(d), and 2(e) show the XRD patterns of samples made in hexadecane at 190 °C, 250 °C, and 285 °C, respectively, and the estimated domain sizes are 13, 17, and 24 Å, respectively. Comparing XRD patterns with the NMR spectra of these samples, a strong correlation can be noticed between the disappearance of the broad resonance peak at 150 ppm and the appearance of resolved (220) and (311) peaks in the XRD patterns. This suggests again that the origin of this broad peak around 150 ppm is disorder. In all samples made in hexadecane a narrow peak around 200 ppm is present. The linewidth of this peak decreases as the temperature of the chemical reaction increases. Furthermore, the two-peak structure, as observed in the flame-annealed sample made in quinoline, also appears in samples made in hexadecane at temperatures above 250 °C. This is illustrated in Fig. 3(d) where spectral details of the ^{71}Ga MAS spectra near the 200 ppm region are shown for the sample synthesized at 280 °C.

Spectra of the nanophase GaAs sample made in trioctyl amine at 290 °C, as illustrated by the ^{71}Ga MAS spectrum shown in Fig. 1(f), were nearly identical to that of the flame-annealed sample made in quinoline. Figures 3(e) and 3(f) display the details of the ^{71}Ga and ^{69}Ga MAS spectra, respectively, near the 200 ppm region. Again, the two-peak structure is present. The determined quadrupole coupling constants and the chemical shifts associated with these two peaks are listed in Table I. The XRD pattern of this sample is shown in Fig. 2(f) from which an average domain size of 30 Å is derived. Shown in Fig. 4 is the ^{75}As MAS spectrum of this sample, where 0 ppm corresponds to the chemical shift of ^{75}As in bulk GaAs. A relatively sharp peak is observed at

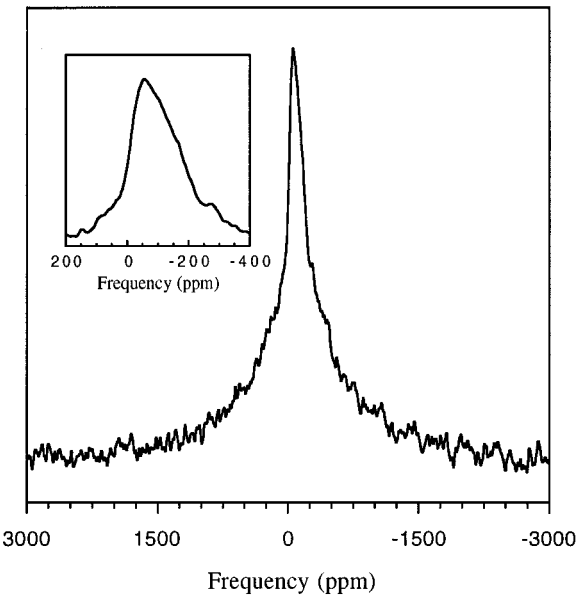

FIG. 4. ^{75}As MAS spectra of GaAs made in trioctyl amine at 290 °C. The inset shows a close-up of the narrow peak at −60 ppm. The spectrum was obtained from the Hahn–echo pulse sequence with a 1.5 μs $\pi/2$ pulse and with a MAS rotation frequency of 16 kHz.

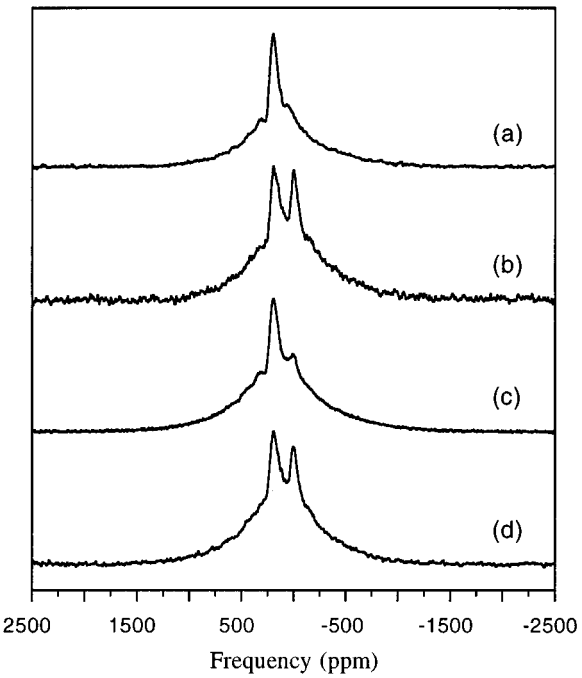

FIG. 5. ^{71}Ga MAS spectra of GaAs made in hexadecane, before and after exposure to air. (a) and (c) are the spectra of the samples made at 100 °C and 190 °C, respectively, before exposure. (b) and (d) are the spectra of the samples made at 100 °C and 190 °C, respectively, after exposure. The spectra were obtained from the Hahn-echo pulse sequence with a 2.3 μs $\pi/2$ pulse and with a MAS rotation frequency of 17 kHz.

-60 ppm together with a broad peak. Since ^{75}As has a much larger quadrupole moment and a lower resonance frequency than both ^{71}Ga and ^{69}Ga, it is very sensitive to lattice defects which destroy the local cubic symmetry of the ideal GaAs structure. The presence of the broad ^{75}As peak is a clear indication of the presence of defects and boundary effects even in samples made at high temperatures. The linewidth $\Delta\nu_{1/2}$ is about 10 kHz for the narrow peak shown in the inset of Fig. 4. If the 10 kHz linewidth is dominated by the residual second-order quadrupolar broadening, then according to powder pattern simulations, the second-order quadrupolar shift δ_i can be as large as -100 ppm. Thus, the isotropic chemical shift of the narrow ^{75}As peak $\delta_c = \delta_e - \delta_i$ can be close to the bulk value.

As mentioned previously, the peak at 0 ppm in the ^{71}Ga and ^{69}Ga spectra arises from oxidation. This point is demonstrated in Fig. 5. Two samples made in hexadecane at 100 °C and 190 °C were sealed in air-tight MAS rotors before exposure to air. The ^{71}Ga MAS spectra of these sealed samples were taken and are shown in Fig. 5(a) and 5(c) for samples made at 100 °C and 190 °C, respectively. The 0 ppm peak is very weak in both cases. The ^{71}Ga MAS spectra were also taken for samples exposed to air. These spectra are shown in Figs. 5(b) and 5(d) for the samples made at 100 °C and 190 °C, respectively. It is very clear that the 0 ppm peak grows significantly stronger in both samples after exposure to air. Based on previous studies of various Ga compounds, the 0 ppm chemical shift is a clear indication of the sixfold-coordinated gallium site in gallium oxide.[24–27] It is important to mention that the two-peak feature, *a* and *b*, is present in samples before air exposure. The spectra in Figs. 1(f), 3(e), and 3(f) were taken from a powder sample made in trioctyl amine sealed in an air-tight MAS rotor before air exposure. As shown in Fig. 1(f), the 0 ppm peak associated with gallium oxide is absent in this sample.

To further characterize the two different Ga environments, spin–lattice relaxation and spin–spin relaxation measurements were carried out. The technique of selective inversion recovery of the central transition was used to determine the spin–lattice relaxation time T_1.[28] The recovery of the magnetization follows a single exponential function in all T_1 measurements discussed here. The value of the spin–lattice relaxation time T_1 for ^{71}Ga is 0.77 s in bulk GaAs at room temperature. Accurate T_1 measurements were carried out for the nanophase GaAs sample made in trioctyl amine. The measured T_1 value for ^{71}Ga is 0.15 s which is shorter than in bulk GaAs. In bulk GaAs the spin–lattice relaxation is dominated by the mechanism of quadrupolar relaxations via couplings to phonons.[29] The reduction of T_1 in nanophase GaAs may result from couplings to dynamic processes near domain boundaries. Peaks *a* and *b* were found to recover with identical rates after inversion under MAS.

The spin–spin relaxation time T_2 was measured systematically for the nanophase GaAs sample made in trioctyl amine using the Hahn-echo technique. The decays of the echo height as a function of the dephasing time 2τ are exponential $[(\propto\exp(-2\tau/T_2)]$ both under static as well as MAS conditions. Peaks *a* and *b*, resolved under MAS, decay with identical rates as a function of 2τ. For ^{71}Ga the T_2 value is 690 μs under the static condition and 1040 μs under MAS; for ^{69}Ga the T_2 value is 848 μs under the static condition and 1380 μs under MAS. Because dipolar interactions are removed under fast MAS,[18] the spin–spin relaxation times should be longer under MAS than under the static condition. It is interesting to note, however, that the reductions of $1/T_2$ values under MAS are less than 50% of that measured under the static condition. Since T_1 values are much larger than T_2, spin–lattice relaxation cannot be responsible for the echo-height decay. Therefore, the mechanism causing the rapid echo-height decay under fast MAS can only originate from strong isotropic indirect couplings.[14,30,31] Strong indirect couplings are usually strong in narrow-gap bulk semiconductors.[22,31] In bulk GaAs, the echo-height decay under fast MAS is dominated by isotropic homonuclear indirect couplings; the influence of isotropic heteronuclear indirect couplings, which are much stronger than homonuclear indirect couplings in bulk GaAs, is removed by the refocusing π pulse to the lowest-order approximation.[23,32] Consequently, the T_2 value measured by the Hahn-echo technique under fast MAS is a measure of the isotropic homonuclear indirect couplings. The isotropic homonuclear indirect coupling J is proportional to the square of the gyromagnetic ratio γ of the observed nuclei.[22,23,30,31] Given that the square root of the second moment M_2 is proportional to $1/T_2$,[14,17,22,23,32] it can be shown easily that the ratio $\sqrt{M_2(^{71}\mathrm{Ga})/M_2(^{69}\mathrm{Ga})}$ is equal to $[\gamma^2(^{71}\mathrm{Ga})/\gamma^2(^{69}\mathrm{Ga})]\sqrt{P(^{71}\mathrm{Ga})/P(^{69}\mathrm{Ga})} = 1.3$ where P is the natural isotopic abundance of the corresponding nucleus. This is in good agreement with the measured T_2 values of 1040 and 1380 μs for ^{71}Ga and ^{69}Ga, respectively.

However, direct comparisons between the T_2 values of the nanophase and bulk GaAs are complicated by the different shapes (Gaussian in bulk GaAs) of the echo-decay curves as a function of the dephasing time. Since isotropic indirect couplings are related to the electronic states through hyperfine interactions,[29,30] the identical T_2 values for peaks *a* and *b* demonstrate again that both peaks originate from similar local environments.

Previous NMR studies of bulk GaAs demonstrate that ^{69}Ga (as well as ^{71}Ga and ^{75}As) spectra are very sensitive to the presence of defects because of the distortion of the cubic symmetry of the zincblende lattice.[33,34] An impurity in bulk GaAs may induce an observable EFG at lattice sites within about 30 Å.[34] Significant quadrupole interactions have also been observed in other materials with cubic symmetry such as NaCl.[35] In nanophase GaAs, for instance, boundaries of domains and defects may cause such quadrupolar broadening. Compared with other studies of gallium nuclei, the less than 1 MHz quadrupole coupling constant (for ^{71}Ga) might be considered as very small, indicating a nearly cubic local symmetry at both local environments associated with peaks *a* and *b*. Clearly, quantitative calculations of EFG tensors and structural models need to be developed for further discussion of lattice distortions.

NMR properties of peak *a* such as the chemical shift and T_2 under MAS are very similar to that in bulk GaAs. Therefore, peak *a* is assigned to gallium sites with a zincblendelike environment. This is consistent with the result of XRD [Fig. 2(b), 2(e), and 2(f)] where the diffraction peaks can be accurately indexed by the (111), (220), and (311) peaks of zincblende GaAs as shown in Fig. 2(g) [for comparison, the calculated XRD spectrum of perfect wurtzite GaAs is shown in Fig. 2(h)]. In contrast, the presence of peak *b* is incompatible with the zincblendelike structure which has only one crystallographic gallium site. Based on the intensity ratio between peaks *a* and *b* nearly half of the ordered region is associated with peak *b*. The spatial proximity between lattice sites associated with peaks *a* and *b* is unclear. However, the nearly identical T_1 and T_2 values of peaks *a* and *b* indicate a close proximity. One of the structural models that is consistent with all observations reported here is the presence of stacking faults which lead to layers with either zincblendelike or wurtzitelike local environments.[3] The assumption that peak *b* originates from wurtzitelike layers is plausible because these atoms are also tetrahedrally coordinated. Theoretical calculations show that zincblende and wurtzite bulk GaAs have nearly identical total energies.[36] Thus, it is not surprising that both kinds of local environments can be found in nanophase GaAs where strains can be relaxed near the domain boundaries. Since bulk GaAs in wurtzite structure is not available, no comparison can be made between peak *b* and the NMR signal in bulk wurtzite GaAs. ZnS exists in both zincblende and wurtzite structures and NMR results are available for both structures. It is interesting to note that the chemical shift of ^{67}Zn nuclei in wurtzite ZnS is shifted about 15 ppm up-field from that of zincblende structure.[37] Although quantum confinement may also cause an up-field shift,[4] the current nanophase GaAs systems do not favor this interpretation as the domains are not isolated from each other.[38] Moreover, different T_1 values would also be expected for peaks *a* and *b* if peak *b* is associated with quantum-confined nanocrystals. The presence of impurities may also change the isotropic chemical shift depending on the impurity level. However, as shown in Figs. 3(b) and 3(e), the two-peak feature of the flame-annealed sample made in quinoline is almost identical to that made in trioctyl amine. This favors the proposal that peak *b* is associated with an intrinsic well-defined local environment. It is not clear whether the presence of the two-peak structure is due to the thermodynamic effect or the kinetics of the growth mechanism.

IV. CONCLUSION

Both NMR and XRD reveal that nanophase GaAs powders synthesized below 250 °C consist mainly of amorphous GaAs materials. Raising the temperature of synthesis (or post-synthesis annealing) above 280 °C improves the crystallinity significantly. This is evidenced both by the narrowing of XRD peaks and the appearance of a sharp bulklike NMR peak. Simultaneously, another sharp NMR peak, which is slightly shifted up-field, also appears. This is incompatible with the bulklike zincblende structure which only has one crystallographic site. The symmetries of the corresponding local environments for the bulklike peak and the peak shifted up-field are very similar. The two peaks also exhibit nearly identical spin–lattice and spin–spin relaxation times. These NMR observations indicate that the structures of nanocrystalline domains in nanophase GaAs undergo a well-defined lattice distortion. A structural model that is consistent with both the NMR and XRD experiments is the presence of stacking faults. Further investigations are needed to clarify the issue. The present work demonstrates that solid-state NMR can provide local structural information about defects in nanocrystals that is difficult to access by XRD.

ACKNOWLEDGMENTS

L.P. and Y.W. acknowledge support from the National Science Foundation under Contract No. DMR-9122992 and from the Petroleum Research Fund under contract ACS-PRF#25902-G3. A.G. and A.P.A. acknowledge support from the Director, Office of Energy Research, Office of Basic Energy Sciences, Materials Science Division, of the US Department of Energy under Contract No. DE-AC03-76SF00098.

[1] See, for example, L. Brus, J. Phys. Chem. **90**, 2555 (1986); M. A. Reed, Sci. Am. **268**, 118 (1993); G. D. Stucky and J. E. MacDougall, Science **247**, 669 (1990); M. G. Bawendi, W. L. Wilson, L. Rothberg, P. J. Carroll, T. M. Jedju, M. L. Steigerwald, and L. E. Brus, Phys. Rev. Lett. **65**, 1623 (1990); L. Brus, Appl. Phys. A **53**, 465 (1991); M. Haase and A. P. Alivisatos, J. Phys. Chem. **96**, 6756 (1992).

[2] C. B. Murry, D. J. Norris, and M. G. Bawendi, J. Am. Chem. Soc. **115**, 8706 (1993).

[3] J.-W. Hwang, J. P. Campbell, J. Kozubowski, S. A. Hanson, J. F. Evans, and W. L. Gladfelter, Chem. Mater. **7**, 517 (1995).

[4] A. M. Thayer, M. L. Steigerwald, T. M. Duncan, and D. C. Douglass, Phys. Rev. Lett. **60**, 2673 (1988).

[5] N. Herron, Y. Wang, and H. Eckert, J. Am. Chem. Soc. **112**, 1322 (1990).

[6] J. R. Sachleben, E. W. Wooten, L. Emsley, A. Pines, V. L. Colvin, and A. P. Alivisatos, Chem. Phys. Lett. **198**, 431 (1992).

[7] L. R. Becerra, C. B. Murray, R. G. Griffin, and M. G. Bawendi, J. Chem. Phys. **100**, 3297 (1994).
[8] M. L. Steigerwald, A. P. Alivisatos, J. M. Gibson, T. D. Harris, R. Kortan, A. J. Muller, A. M. Thayer, T. M. Duncan, D. C. Douglass, and L. E. Brus, J. Am. Chem. Soc. **110**, 3046 (1988).
[9] R. L. Wells, C. G. Pitt, A. T. McPhail, A. P. Purdy, S. Shafieezad, and R. B. Hallock, Chem. Mater. **1**, 4 (1989).
[10] M. A. Olshavsky, A. N. Goldstein, and A. P. Alivisatos, J. Am. Chem. Soc. **112**, 9438 (1990).
[11] H. Uchida, C. J. Curtis, P. V. Kamat, K. M. Jones, and A. J. Nozik, J. Phys. Chem. **96**, 1156 (1992).
[12] L. Butler, G. Redmond, and D. Fitzmaurice, J. Phys. Chem. **97**, 10750 (1993).
[13] S. S. Kher and R. L. Wells, Chem. Mater. **6**, 2056 (1994).
[14] C. P. Slichter, *Principles of Magnetic Resonance* (Springer-Verlag, Berlin, 1990).
[15] P. P. Man, J. Klinowski, A. Trokiner, H. Zanni, and P. Papon, Chem. Phys. Lett. **151**, 143 (1988).
[16] A. Guinier, *X-Ray Diffraction* (Freeman, San Francisco, 1963).
[17] D. Freude and J. Haase, NMR Basic Principles Progress **29**, 1 (1993).
[18] U. Haeberlen, *High Resolution NMR in Solids* (Academic, New York, 1976).
[19] A. Samoson, E. Kundla, and E. Lippmaa, J. Magn. Reson. **49**, 350 (1982).
[20] S. Ganapathy, S. Schramm, and E. Oldfield, J. Chem. Phys. **77**, 4360 (1982).
[21] K. T. Mueller, Y. Wu, and B. F. Chmelka, J. Am. Chem. Soc. **113**, 32 (1991).
[22] R. K. Sundfors, Phys. Rev. **185**, 458 (1969).
[23] L. D. Potter and Y. Wu, J. Magn. Reson. (in press).
[24] J. Zhong and P. J. Bray, J. Non-Cryst. Solids **94**, 122 (1987).
[25] H. Timken and E. Oldfield, J. Am. Chem. Soc. **109**, 7669 (1987).
[26] A. P. M. Kentgens, C. R. Bayense, J. H. C. van Hooff, J. W. de Haan, and L. J. M. van de Ven, Chem. Phys. Lett. **176**, 399 (1991).
[27] F. Miyaji, K. Tadanaga, T. Yoko, and S. Sakka, J. Non-Cryst. Solids **139**, 268 (1992).
[28] E. R. Andrew and D. P. Tunstall, Proc. Phys. Soc. **78**, 1 (1961).
[29] J. A. McNeil and W. G. Clark, Phys. Rev. B **13**, 4705 (1976).
[30] P. W. Anderson, Phys. Rev. **99**, 623 (1955).
[31] R. G. Shulman, J. M. Mays, and D. W. McCall, Phys. Rev. **100**, 692 (1955).
[32] M. Engelsberg and R. E. Norberg, Phys. Rev. B **5**, 3395 (1972).
[33] E. H. Rhoderick, J. Phys. Chem. Solids **8**, 498 (1958).
[34] W. E. Carlos and S. G. Bishop, Phys. Rev. B **43**, 12512 (1991).
[35] R. E. Slusher and E. L. Hahn, Phys. Rev. **166**, 332 (1968).
[36] S. Froyen and M. L. Cohen, Phys. Rev. B **28**, 3258 (1983).
[37] T. J. Bastow and S. N. Stuart, Phys. Stat. Sol. (b) **145**, 719 (1988).
[38] The spectrum of isolated GaAs nanoparticles is significantly different from the one reported here, Y. Wu, L. D. Potter, S. Kher, and R. L. Wells, unpublished results.